frontiers | Frontiers in Medicine

TYPE Original Research
PUBLISHED 06 October 2022
DOI 10.3389/fmed.2022.881848

OPEN ACCESS

EDITED BY
Luigi M. Terracciano,
University of Basel, Switzerland

REVIEWED BY
Max Petersen,
Washington University in St. Louis, United States
Henricus A. M. Mutsaers,
Aarhus University, Denmark

*CORRESPONDENCE
Jennifer Y. Chen
Jennifer.Chen4@ucsf.edu

†These authors have contributed equally to this work and share first authorship

‡These authors have contributed equally to this work and share last authorship

SPECIALTY SECTION
This article was submitted to Pathology, a section of the journal Frontiers in Medicine

RECEIVED 23 February 2022
ACCEPTED 15 September 2022
PUBLISHED 06 October 2022

CITATION
Yu A, Cable C, Sharma S, Shihan MH, Mattis AN, Mileva I, Hannun YA, Duwaerts CC and Chen JY (2022) Targeting acid ceramidase ameliorates fibrosis in mouse models of non-alcoholic steatohepatitis. *Front. Med.* 9:881848. doi: 10.3389/fmed.2022.881848

Targeting acid ceramidase ameliorates fibrosis in mouse models of non-alcoholic steatohepatitis

Amy Yu[1†], Carson Cable[1†], Sachin Sharma[1], Mahbubul H. Shihan[1], Aras N. Mattis[2,3], Izolda Mileva[4], Yusuf A. Hannun[4], Caroline C. Duwaerts[1,3‡] and Jennifer Y. Chen[1,3*‡]

[1]Department of Medicine, University of California, San Francisco, San Francisco, CA, United States, [2]Department of Pathology, University of California, San Francisco, San Francisco, CA, United States, [3]The Liver Center, University of California, San Francisco, San Francisco, CA, United States, [4]Department of Medicine and Biochemistry and the Stony Brook Cancer Center, Stony Brook University, Stony Brook, NY, United States

Non-alcoholic fatty liver disease (NAFLD) is a common cause of liver disease worldwide, and is characterized by the accumulation of fat in the liver. Non-alcoholic steatohepatitis (NASH), an advanced form of NAFLD, is a leading cause of liver transplantation. Fibrosis is the histologic feature most associated with liver-related morbidity and mortality in patients with NASH, and treatment options remain limited. In previous studies, we discovered that acid ceramidase (aCDase) is a potent antifibrotic target using human hepatic stellate cells (HSCs) and models of hepatic fibrogenesis. Using two dietary mouse models, we demonstrate that depletion of aCDase in HSC reduces fibrosis without worsening metabolic features of NASH, including steatosis, inflammation, and insulin resistance. Consistently, pharmacologic inhibition of aCDase ameliorates fibrosis but does not alter metabolic parameters. The findings suggest that targeting aCDase is a viable therapeutic option to reduce fibrosis in patients with NASH.

KEYWORDS

acid ceramidase, non-alcoholic fatty liver disease, hepatic fibrosis, hepatic stellate cell, glucose tolerance

Introduction

Characterized by progressive matrix stiffening, tissue fibrosis is a leading cause of morbidity and mortality (1). Despite steady progress in basic, translational, and clinical research of fibrogenesis, there remain limited treatment options for patients. Organ transplantation is an effective option for end-stage disease, but is limited by

donor organ availability. This underscores the need for new therapies for patients with fibrotic diseases.

The burden of end-stage liver disease has risen significantly due to the increasing global prevalence of non-alcoholic fatty liver disease (NAFLD). NAFLD is characterized by the accumulation of lipids within hepatocytes, and is associated with features of metabolic syndrome such as obesity, insulin resistance, and hyperlipidemia. NAFLD represents a spectrum of liver disease that can lead to progressive non-alcoholic steatohepatitis (NASH), fibrosis, and ultimately hepatocellular carcinoma (HCC) and liver failure. Among patients with NASH, fibrosis is the histologic measure that predicts liver-related mortality (2), further highlighting the need for antifibrotic therapies.

Hepatic stellate cells (HSCs) drive liver fibrosis, and our prior studies identified a new antifibrotic target, acid ceramidase (aCDase) (3), an enzyme responsible for ceramide hydrolysis. We demonstrated that targeting aCDase promotes HSC inactivation (3). In additional studies, we showed that genetic deletion in HSCs or pharmacologic inhibition of aCDase ameliorates fibrosis in mouse models. Mechanistically, we illustrated that targeting aCDase inhibits YAP/TAZ activity by potentiating its proteasomal degradation. We also demonstrated that aCDase inhibition reduces fibrogenesis in human fibrotic precision-cut liver slices. Consistently, patients with advanced fibrosis have increased aCDase expression compared to those with mild fibrosis (4). Furthermore, a signature of the genes most downregulated by ceramide, the ceramide responsiveness score (CRS), identifies patients with advanced fibrosis who could benefit from aCDase targeting (4).

Given the rising prevalence of NAFLD and the lack of available therapies, we aimed to determine how targeting aCDase regulates fibrosis and metabolic parameters in mouse models of NASH. These studies are particularly relevant, as others have shown that ceramide species can contribute to insulin resistance and steatosis (5–10), which would complicate NASH treatment. We previously observed that genetic depletion of aCDase in HSCs ameliorates fibrosis development without altering steatosis in one model of NASH, the choline-deficient L-amino acid-defined, high-fat diet (CDAHFD) model (4). Here, we aimed to characterize the effect of targeting aCDase on metabolic parameters in the CDAHFD model and in a second dietary model of NASH, the Fructose, Palmitate, and Cholesterol (FPC) model. In this study, we demonstrate that genetic deletion in HSCs or pharmacologic inhibition of aCDase reduces fibrosis but does not worsen metabolic parameters of NASH. This work highlights the therapeutic potential of aCDase targeting in patients with NASH.

Materials and methods

Animals

Animal experiments were approved by the Institutional Animal Care and Use Committee at the University of California, San Francisco. All animals received humane care according to the criteria outlined in the *Guide for the Care and Use of Laboratory Animals of the National Academy of Sciences*.

To generate the HSC depletion of aCDase, we crossed *Asah1*$^{flox/flox}$ (provided by Lina Obeid) (11) with *Pdgfrb*-Cre (12) (*Asah1*^{cko}, cACKO). Control mice were *Asah1*$^{flox/flox}$ lacking *Pdgfrb*-Cre. In the CDAHFD model, 6- to 8-week-old male mice received either normal chow (PicoLab Rodent Diet 20; LabDiet #5053) or CDAHFD (L−amino acid diet with 60 kcal% fat with 0.1% methionine without added choline; Research Diets A06071302) *ad libitum* for 14 weeks. In the FPC model, 6- to 8-week-old sex-matched mice received either normal chow or FPC (Envigo TD 160785) supplemented with high fructose drinking water (45:55 fructose:glucose) *ad libitum* for 16 weeks (13). Mice were weighed and food consumption measured once a week. Weekly food intake was measured by monitoring the weight difference between added food and the remaining food.

For the therapeutic B13 experiment, male C57BL/6J mice (age 6–8 weeks, Jackson Laboratory, Bar Harbor, ME, USA) received FPC diet *ad libitum* for 9 weeks. Mice then received either 50 mg/kg B13 or vehicle 5 days/week by IP for 3 weeks (total weeks on the FPC diet = 12 weeks).

A terminal blood collection was performed by cardiac puncture. Livers were weighed and were subsequently fixed in formalin or 4% paraformaldehyde or were snap frozen. Mice were fasted for 4 h prior to sacrifice.

Serum analysis

Harvested blood was processed for collection of serum. Serum was used to measure ALT and total cholesterol at Zuckerberg San Francisco General Hospital. The insulin ELISA was performed on mouse serum according to the manufacturer instructions for the "Low Range Assay" of the kit (Crystal Chem, Ultra Sensitive Mouse Insulin ELISA Kit #90080).

Hepatic triglycerides

Lipids were extracted from liver tissue using the Folch method (14). Liver triglycerides were quantified as described previously (15).

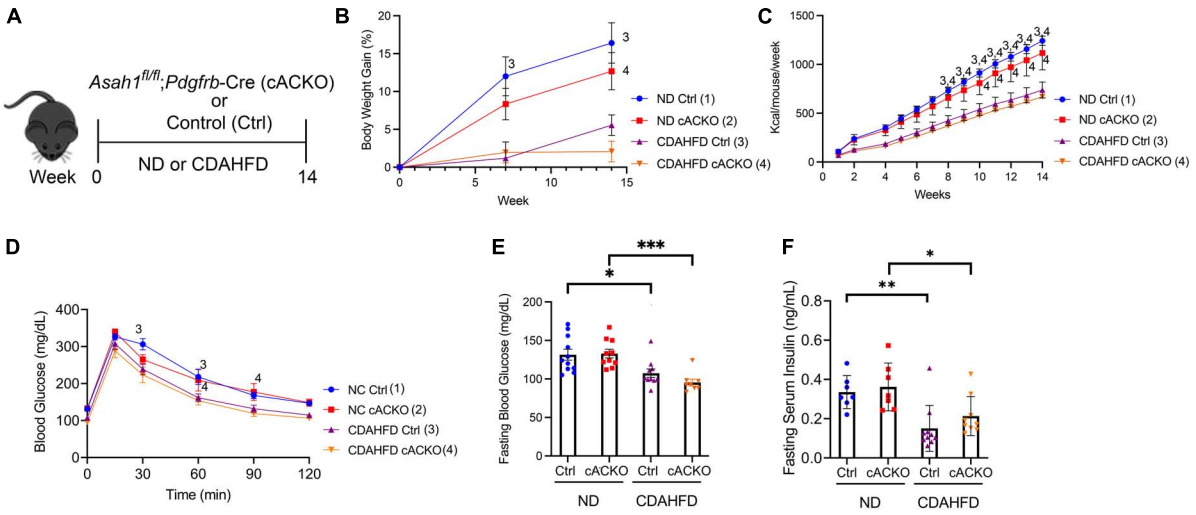

FIGURE 1
Hepatic stellate cell-specific acid ceramidase knockout mice on a CDAHFD demonstrate no metabolic differences compared with their wild-type counterparts. **(A)** Experimental schematic. Male and female hepatic stellate cell-specific acid ceramidase knockout mice (cACKO) or control (Ctrl) mice were fed either normal diet (ND) or CDAHFD for 14 weeks. **(B)** Body weight percent over time. **(C)** Food intake in Kcal/mouse/week. **(D)** Glucose tolerance test. **(E)** Fasting blood glucose levels measured at 14 weeks. **(F)** Fasting serum insulin levels measured at 14 weeks. n = 8–11 mice per group. $^{*}p < 0.05$, $^{**}p < 0.01$, $^{***}p < 0.001$, $^{1\text{-}4}p < 0.05$ to the corresponding group number.

Sphingolipid analysis

Sphingolipid analysis was performed as described previously using LC/MS/MS (3).

Glucose tolerance test

Mice were fasted for 5 h before blood was collected from the base of the tail. Glucose was measured using a glucometer (Accu-Chek Performa Nano #06454283056). Blood glucose was measured at start of test (0 min time-point). Mice then received 20% glucose solution via intraperitoneal (IP) injection (10 μL per gram of weight), and glucose measurements were taken at the following time points after IP injection: 15, 30, 60, 90, and 120 min.

Histology, Sirius red staining, immunofluorescence, and immunohistochemistry

Formalin-fixed samples were embedded in paraffin, cut in 5 μm sections, and stained with hematoxylin & eosin (H&E) by Peninsula Histopathology Laboratory. Sirius red staining was performed as previously described (12). The collagen proportional area (CPA) was morphometrically quantified on Sirius red-stained sections with ImageJ as previously described (12). Slides were evaluated by a blinded expert UCSF liver pathologist (ANM) for steatosis and lobular inflammation using a histological scoring system for NAFLD (16).

For immunofluorescence (IF) staining of type 1 collagen, formalin-fixed, paraffin-embedded (FFPE) mouse liver tissues were prepared in 5 μm sections. FFPE sections were deparaffinized and hydrated in water. Heat-induced epitope retrieval (HIER) was carried out using 10 mM sodium citrate buffer (pH- 6.0 with 0.05% Tween-20) (Sigma-Aldrich, #C8532). Blocking was performed with 5% normal donkey serum for 1 h (Jackson ImmunoResearch #017-000-121). Collagen I primary antibody (1:100 dilution; Signaling Technology, #72026) was then incubated overnight at 4°C diluted in 5% donkey serum (Jackson ImmunoResearch, #017-000-121). After incubation, the liver tissue was washed three times with 1X PBS and incubated with Alexa Fluor 488 fluorochrome-conjugated secondary (Invitrogen, # A-11034) for 1 h at room temperature. The tissue was washed three times with 1X PBS, incubated with DAPI (2 μg/ml, ThermoFisher Scientific, #D1306) at room temperature, and mounted with antifade mounting media (Invitrogen, # P36981). Images were acquired with Zeiss LSM 780 microscope at 10× magnification. Quantification of three random fields per section of sample was conducted using ImageJ. Mean fluorescence intensity (MFI) was measured for each sample per group.

For immunohistochemistry (IHC) staining, 5 μm liver tissue sections were deparaffinized and water hydrated followed by HIER using 10 mM sodium citrate buffer as described above. The liver tissue was blocked with BLOXALL blocking solution (Vector Laboratories, #SP-6000) for 10 min, washed three

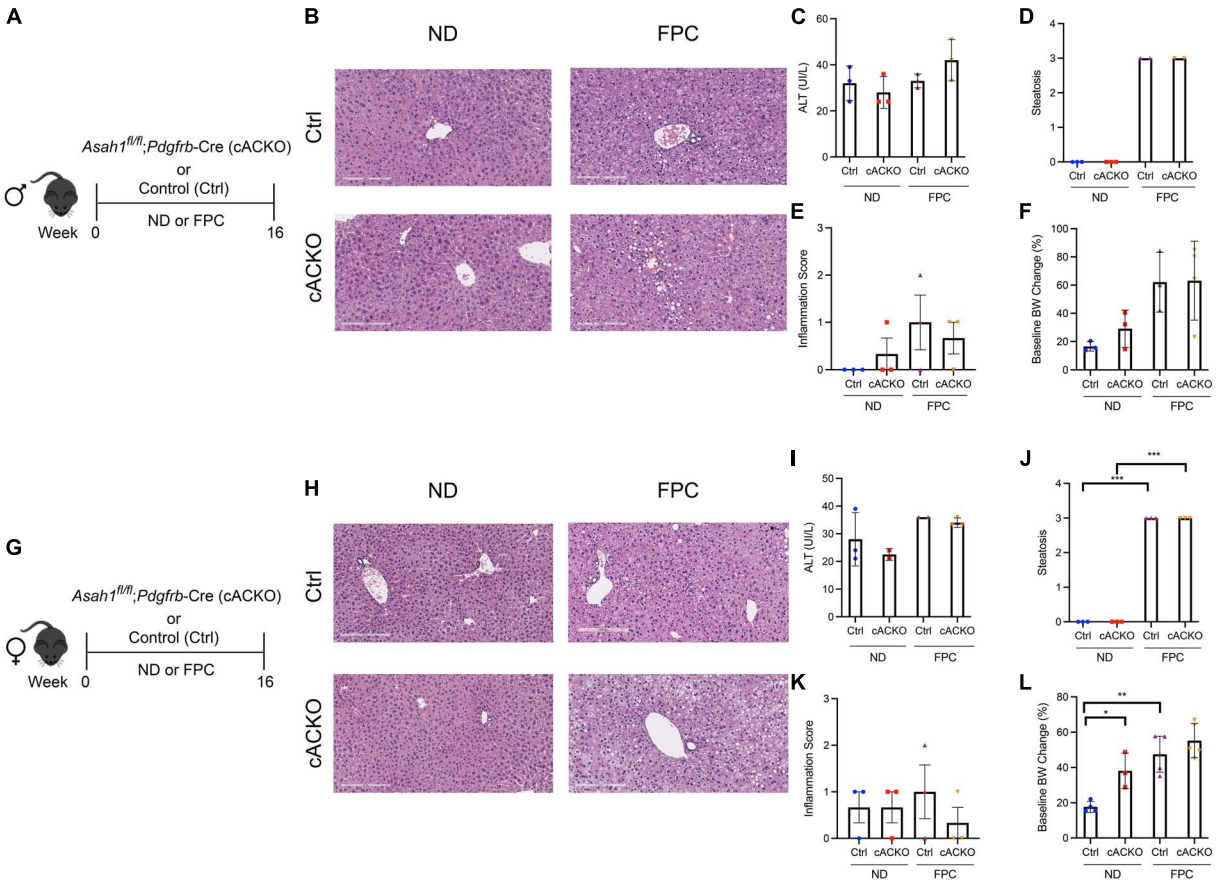

FIGURE 2
Hepatic stellate cell-specific acid ceramidase knockout mice on a FPC diet demonstrate no liver or metabolic differences compared with their wild-type counterparts. **(A,G)** Experimental schematic. Male and female hepatic stellate cell-specific acid ceramidase knockout mice (cACKO) or control (Ctrl) mice were fed either normal diet (ND) or Fructose, Palmitate, and Cholesterol diet (FPC) for 16 weeks. **(B,H)** Representative photomicrograph of H&E-stained liver sections. **(C,I)** Measured serum ALT levels. **(D,J)** Liver steatosis graded by a blinded pathologist. **(E,K)** Inflammation score graded by a blinded pathologist. **(F,L)** Body weight (BW) percent change at 16 weeks post-diet from start weight. $n = 2–6$ mice per group. $^{*}p < 0.05$, $^{**}p < 0.01$, $^{***}p < 0.001$.

times with 1X PBS, and blocked using 5% normal goat serum (Jackson ImmunoResearch, #005-000-121) for 1 h at room temperature. The liver tissue was incubated with Avidin/Biotin Blocking reagent (Vector Laboratories, #SP-2001) for 15 min and incubated overnight at 4°C with anti-galectin-3 (Mac2) primary antibody (1:100; Santa Cruz, #SC-20157) diluted in 5% normal goat serum. The liver tissue was washed three times with 1X PBS and incubated with biotinylated Secondary antibody (Invitrogen, #B2770) for 1 h at room temperature. The liver tissue was washed three times with 1X PBS, incubated with VECTASTAIN Elite ABC reagent (Vector Laboratories, #PK-6100) for 30 min, and incubated with ImmPACT DAB (Vector Laboratories, #SK-4105) for 1–2 min. The liver tissue was then counterstained with Hematoxylin and mounted with Permount (FisherChemical, #SP15). Three random fields per section images were acquired with Leica X microscope at 20×. ImageJ was used for the quantification and percentage of Mac2 positive cells per microscopic field were calculated for each sample per group.

Quantitative polymerase chain reaction analysis

RNA was isolated from liver tissue using TRIzol (Life Technologies) according to the manufacturer's instructions and then treated with DNAse I (Promega). Total RNA (1 μg) from each sample was reverse transcribed with iScript (Bio-Rad). Power SYBR Green master mix (Life Technologies) was used for quantification of cDNA on a CFX384 Real Time System (Bio-Rad). The following primers were used: forward *Il1b*, 5′-TGCCACCTTTTGACAGTGATG-3′, reverse *Il1b*, 5′-TGATGTGCTGCTGCGAGATT-3′, forward *Cd11b*,

5′-GCCTGTGAAGTACGCCATCT-3′, reverse *Cd11b*, 5′-GCCCAGGTTGTTGAACTGGT-3′, forward *Mcp1*, 5′-CAC TCACCTGCTGCTACTCA-3′, reverse *Mcp1*, 5′-GCTTGG TGACAAAAACTACAGC-3′, forward *F4/80*, 5′-TCACCTT GTGGTCCTAACTCAG-3′, reverse *F4/80*, 5′-TCAGACACT CATCAACATCTGCG-3′, forward *Gapdh*, 5′-AGGTCGGTG TGAACGGATTTG-3′, reverse *Gapdh*, 5′-TGTAGACCA TGTAGTTGAGGTCA-3′.

Statistics

Statistical analysis was performed using GraphPad Prism 8 with unpaired two-sided Student's *t*-tests, one-way ANOVA with Tukey's method for multiple comparisons, or Kruskal–Wallis test with Dunn's multiple comparisons test. Statistical significance was defined as $p < 0.05$.

Results

Hepatic stellate cell depletion of acid ceramidase does not worsen metabolic features in the choline-deficient L-amino acid-defined, high-fat diet model of non-alcoholic steatohepatitis

In previous studies, we demonstrated that HSC deletion of aCDase reduces fibrosis development in the CDAHFD model of NASH (4). Among mice fed CDAHFD, we did not observe significant differences in the development of steatosis, lobular inflammation, or hepatic triglyceride levels between mice with HSC deletion of aCDase and their Cre-negative littermate controls (4).

Here, we explored how HSC deletion of aCDase regulates metabolic parameters of NASH in the CDAHFD model (**Figure 1A**). There was, as expected, an overall significant decrease in weight gain for mice on CDAHFD combined with a significant decrease in food intake (**Figures 1B,C**). Also as expected with this dietary model, the mice experienced no insulin resistance as demonstrated by a normal glucose tolerance test (GTT) (**Figure 1D**). At the time of sacrifice, mice receiving CDAHFD experienced significantly decreased fasting blood glucose and insulin levels compared to those receiving standard chow diet, but there were no significant differences between mice receiving CDAHFD (**Figures 1E,F**). This suggests that although the CDAHFD model produces fibrosis, steatosis, lobular inflammation, and increases in hepatic triglycerides, this model does not recapitulate the weight gain or insulin resistance observed in patients with NASH and thus represents a suboptimal mouse model.

Hepatic stellate cell depletion of acid ceramidase does not worsen metabolic features in the fructose, palmitate, and cholesterol model of non-alcoholic steatohepatitis

To address the limitations of the CDAHFD model, we next utilized the FPC model of NASH, which has been shown to induce insulin resistance after 16 weeks. (13). The FPC model was previously studied in male mice (13), and we sought to decipher whether there were sex-specific differences among mice with HSC deletion of aCDase in the development of fibrosis and features of metabolic syndrome (**Figures 2A,G**).

Female mice receiving the FPC diet experienced significant increases in hepatic steatosis and weight gain compared to mice receiving the standard chow diet (**Figures 2J,L**), and a similar trend was observed among male mice (**Figures 2D,F**). Among male and female mice receiving the FPC diet, there were no significant differences between the conditional knockout mice and control mice with respect to ALT, steatosis, inflammation, and weight gain (**Figures 2B–F,H–L**).

Male mice with hepatic stellate cell depletion of acid ceramidase trend toward decreased fibrosis compared to control male mice

Consistent with our prior data using the CDAHFD model (4), male mice with HSC deletion of aCDase had significantly decreased fibrosis compared to control mice receiving FPC as measured by CPA (**Figures 3A–C**). We did not observe significant differences among female mice receiving the FPC diet (**Figures 3D–F**), suggesting there may be sex differences that modulate this response.

Hepatic stellate cell depletion of acid ceramidase does not worsen metabolic parameters of non-alcoholic steatohepatitis in male mice

Intrigued by these sex-specific differences, we next aimed to characterize metabolic parameters in the conditional knockout mice according to sex. Among male mice, the FPC diet induced significant increases in hepatic triglycerides, liver proportional weight, and serum cholesterol, but there were no significant differences between FPC-fed conditional knockout mice and control mice (**Figures 4A–D**). We observed consistent findings among the female mice (**Supplementary Figures 1A–C**).

In contrast to the CDAHFD model, we observed increases in glucose intolerance among male mice receiving FPC compared

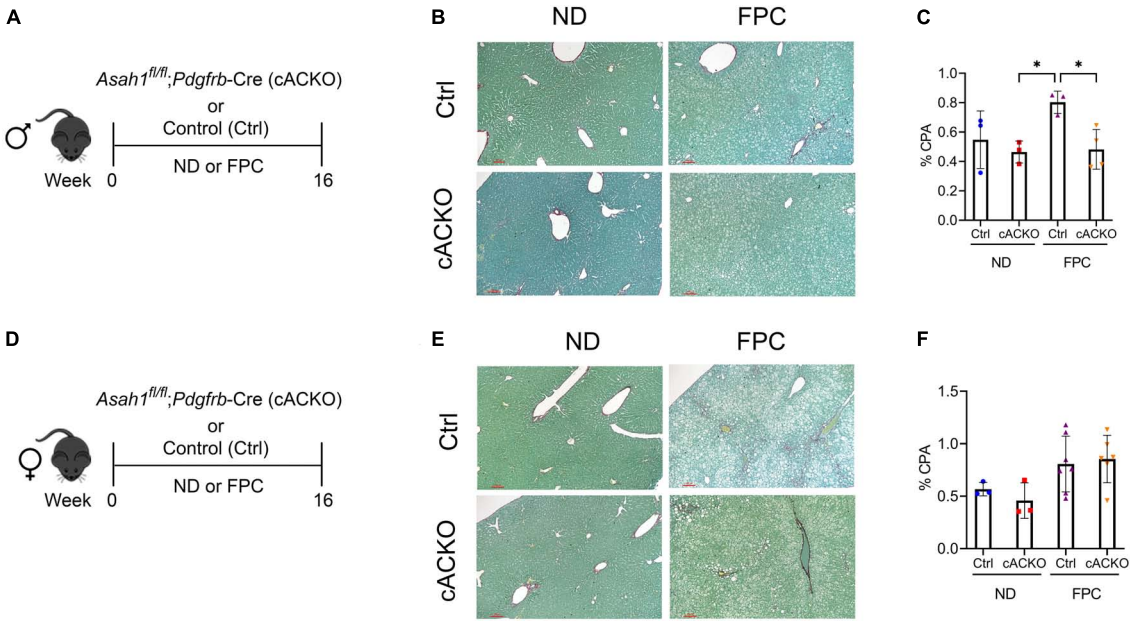

FIGURE 3
Male hepatic stellate cell-specific acid ceramidase knockout mice on a FPC diet develop significantly less fibrosis than wild-type counterparts. **(A,D)** Experimental schematic. Male or female mice of either hepatic stellate cell-specific acid ceramidase knockout (cACKO) or their respective Cre-negative littermate controls (Ctrl) received either normal diet (ND) or Fructose, Palmitate, and Cholesterol (FPC) for 16 weeks. **(B,E)** Representative photomicrograph of Sirius red staining for either male (top) or female (bottom) mice. **(C,F)** Quantification of positive collagen proportional area (Sirius red staining, % CPA) for males (top) or females (bottom). n = 3–6 mice per group. $^{*}p < 0.05$.

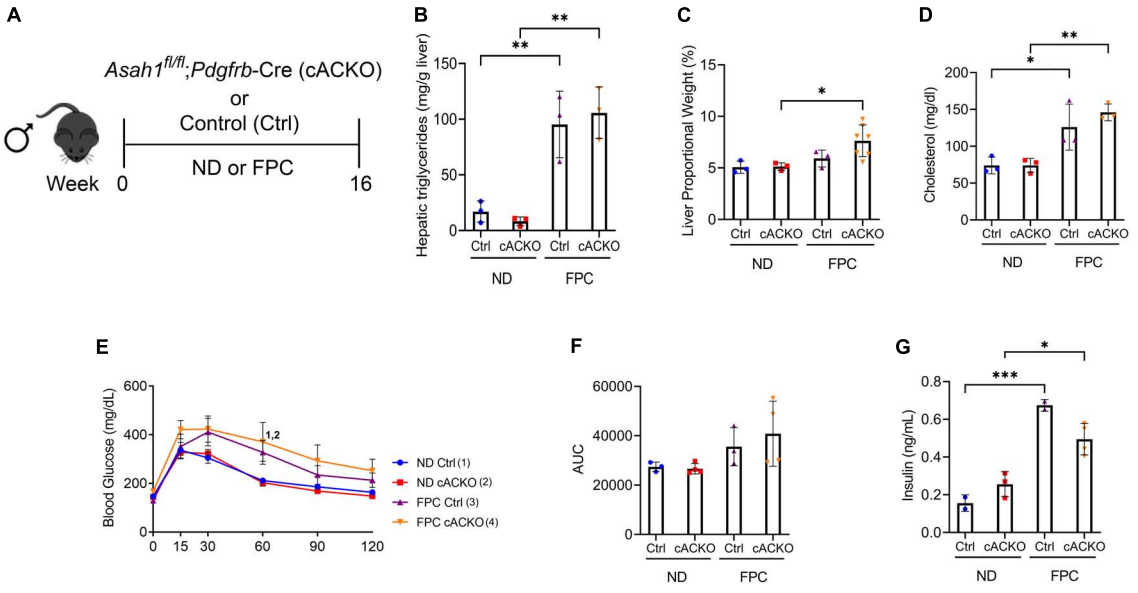

FIGURE 4
Male hepatic stellate cell-specific acid ceramidase knockout mice demonstrate no metabolic differences from their wild-type counterparts. **(A)** Experimental schematic. Male hepatic stellate cell-specific knockout (cACKO) or control (Ctrl) mice were fed either a normal diet (ND) or Fructose, Palmitate, and Cholesterol (FPC) diet for 16 weeks. **(B)** Measured hepatic triglycerides. **(C)** Liver to body proportional weight in percent. **(D)** Measured serum cholesterol levels. **(E,F)** Glucose tolerance test was performed at 14 weeks and area under the curve (AUC) was determined. **(G)** Measured serum insulin levels. n = 3–4 mice per group. $^{*}p < 0.05$, $^{**}p < 0.01$, $^{***}p < 0.001$, $^{1\text{-}4}p < 0.05$ to the corresponding group number.

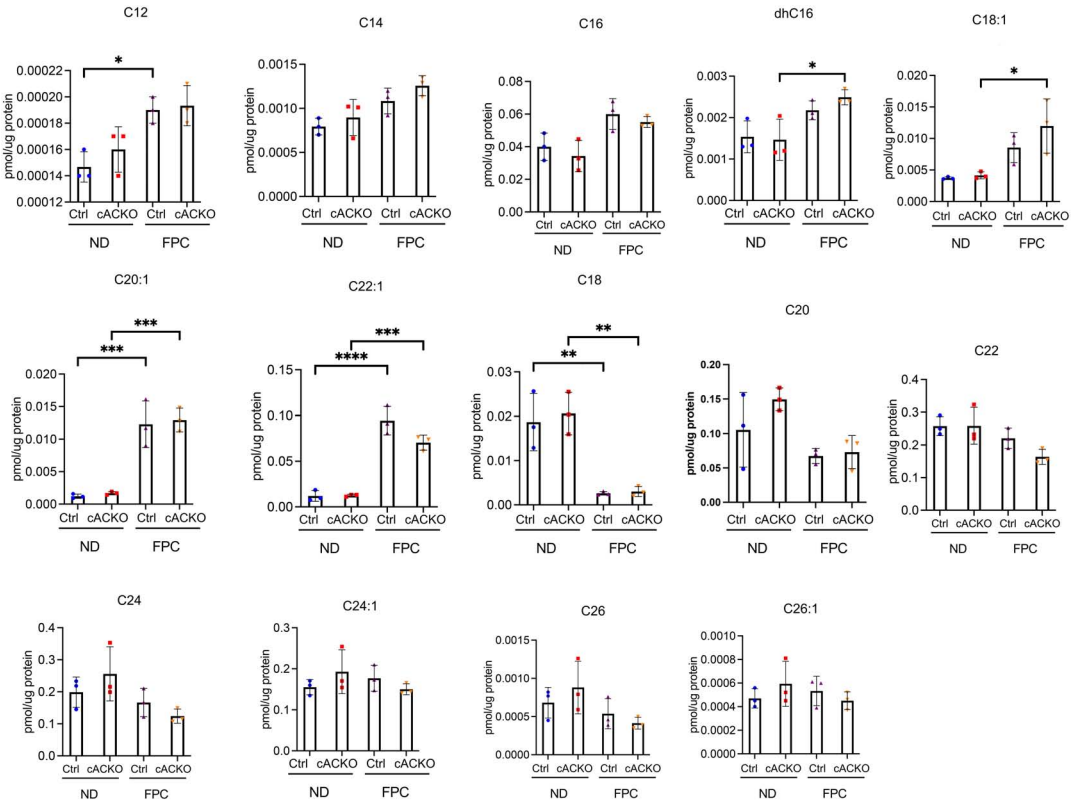

FIGURE 5
Ceramide species were analyzed in male hepatic stellate cell-specific acid ceramidase knockout mice or littermate controls in the FPC model of NASH. Hepatic ceramide subspecies. n = 3–4 mice per group. *$p < 0.05$, **$p < 0.01$, ***$p < 0.001$, ****$p < 0.0001$.

to standard chow diet as measured by a GTT. There were no significant differences among FPC-fed mice (Figures 4E,F). Interestingly, we observed a trend toward a decrease in fasting serum insulin among FPC-fed conditional knockout male mice compared to control mice (Figure 4G), which was not seen in female mice (Supplementary Figures 1D–F).

To measure changes in ceramide subspecies, we performed sphingolipid analysis of liver tissues (Figure 5). This analysis was performed on male mice as we observed a decrease in fibrosis in this group only. We observed that the FPC diet significantly increased C20:1 and C22:1 compared to normal diet. We also observed that the FPC significantly decreased C18. However, there were no significant differences in ceramide subspecies between control and conditional knockout mice receiving normal or FPC diet (Figure 5).

Pharmacologic inhibition of acid ceramidase ameliorates fibrosis and does not worsen metabolic parameters

Our studies thus far have analyzed the role of HSC deletion of aCDase in mouse models of NASH, but the impact of systemic aCDase inhibition has not been elucidated. To further investigate the effect of targeting aCDase for the treatment of NASH, we utilized a pharmacologic inhibitor, B13. B13 has been validated as an aCDase inhibitor in other cell and model systems (17–22), including by our group (4). We next explored how B13 treatment regulates fibrogenesis in the FPC model. We established the NASH phenotype by providing 6–8 weeks old male C57BL/6 mice FPC diet for 9 weeks. Mice then received either B13 or vehicle for an extra 3 weeks while still on diet (total weeks on FPC diet = 12 weeks) (Figure 6A). Given our observation of sex-specific differences in the development of fibrosis using the FPC model, we included only male mice in this analysis.

Receipt of FPC diet significantly increased steatosis, lobular inflammation, and weight gain, but there were no significant differences between FPC-fed mice receiving B13 or vehicle (Figures 6B–E). We did not observe significant changes in ALT level (Figure 6F). The liver proportional weight was lower among FPC-fed mice receiving B13 compared with vehicle (Figure 6G). There were no significant differences in serum fasting blood glucose levels (Figure 6H). The FPC diet induced a significant increase in glucose intolerance among B13-treated mice as measured by glucose tolerance testing

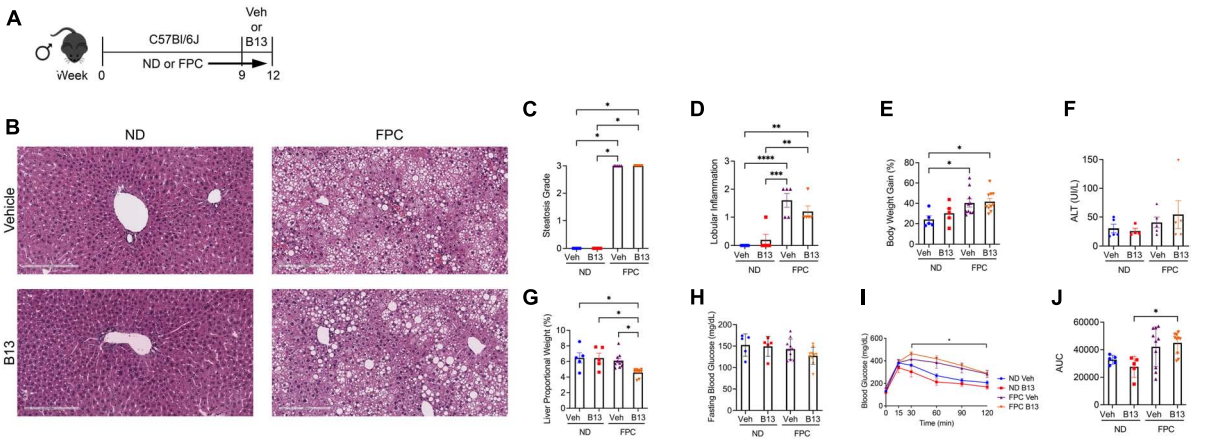

FIGURE 6
Male wild-type mice on FPC diet and administered an acid ceramidase inhibitor developed similar metabolic differences compared with mice receiving vehicle. **(A)** Experimental schematic. Male wild-type mice received either normal diet (ND) or Fructose, Palmitate, and Cholesterol (FPC) diet for a total of 12 weeks. During the last 3 weeks of feeding, they also received either a small molecule acid ceramidase inhibitor (B13, dosed at 50 mg/kg by intraperitoneal injection five times per week) or vehicle control (Veh). **(B)** Representative photomicrograph of H&E-stained liver sections. A pathologist graded **(C)** liver steatosis and **(D)** lobular inflammation. **(E)** Percent body weight gain from start. **(F)** Measured serum ALT levels. **(G)** Liver to body weight proportional weight in percent. **(H)** Fasting blood glucose levels were measured at week 12. **(I,J)** Glucose tolerance test was performed at week 10 and area under the curve (AUC) was calculated. n = 5–10 mice per group. $^{*}p < 0.05$, $^{**}p < 0.01$, $^{***}p < 0.001$, $^{****}p < 0.0001$.

(Figures 6I,J). However, among FPC-fed mice receiving B13 or vehicle, there were no significant differences in glucose intolerance (Figures 6I,J).

Notably, in the FPC model, B13 significantly reduced fibrosis as measured by CPA (Figure 7A) and by type 1 collagen immunofluorescence staining (Figure 7B). We also measured markers of inflammation. Mice receiving the FPC diet had increased Mac-2 staining compared to those on normal diet. Among mice fed the FPC diet, the administration of B13 significantly decreased Mac-2 staining (Figure 7C). Consistent with these findings, we observed an increase in expression of *Cd11b* and *F4/80* among mice receiving the FPC diet compared to those receiving normal diet. Among FPC-fed mice, B13 administration significantly reduced *Cd11b* and *F4/80* expression compared to vehicle (Figure 7D). These data suggest that B13 treatment reduces overall hepatic inflammation.

We also observed decreases in Mcp1 expression among mice receiving FPC diet compared to normal diet, but there were no differences between B13 and vehicle treatment. We observed an increase in *Il1b* expression among mice receiving the FPC diet compared to normal diet, but there were no differences between B13 and vehicle treatment (Figure 7D).

Furthermore, we performed sphingolipid analysis of liver tissues (Figure 8). Consistent with our prior sphingolipid data (Figure 5), we observed that the FPC significantly increased C20:1 and C22:1. We also observed that the FPC increased C16, C26, dhC18, dhC18:1, dhC20, dhC20:1, dhC22, and dhC22:1. Interestingly, several ceramide subspecies significantly decreased with the FPC diet, such as C18 and C24:1. Among mice fed normal diet, B13 treatment significant reduced C24:1 and C26:1. Among mice fed FPC diet, there was a significant decrease in C20:1 with B13 treatment compared to vehicle. Taken together, our findings demonstrate that pharmacologic inhibition of aCDase reduces fibrosis without altering metabolic parameters in the FPC model of NASH.

Discussion

The burden of NAFLD is rising globally, and there are limited treatment options available for patients. In particular, there are no treatment options targeting fibrosis, which drives liver-related morbidity and mortality (2). Our studies suggest that genetic deletion of aCDase in HSCs or pharmacologic inhibition of aCDase ameliorates fibrosis without worsening metabolic features of NASH. This suggests that targeting aCDase represents an effective strategy to reduce fibrosis in this disease setting.

Ceramides constitute a family of sphingolipids that consist of sphingosine linked to a fatty acid, and are generated through several pathways, including *de novo* synthesis from serine and palmitate, sphingomyelin hydrolysis, or recycling of sphingosine. Ceramide species can regulate diverse cellular behavior (23), and ceramide metabolism has been implicated in the pathogenesis of insulin resistance and steatosis (5–10), though the literature is conflicting. Inhibition of *de novo* synthesis, including targeting dihydroceramide desaturase (DES1), mitigates NASH phenotypes (6, 24, 25). Human lipidomic studies have also demonstrated a correlation between insulin resistance and hepatic ceramides (26, 27). However,

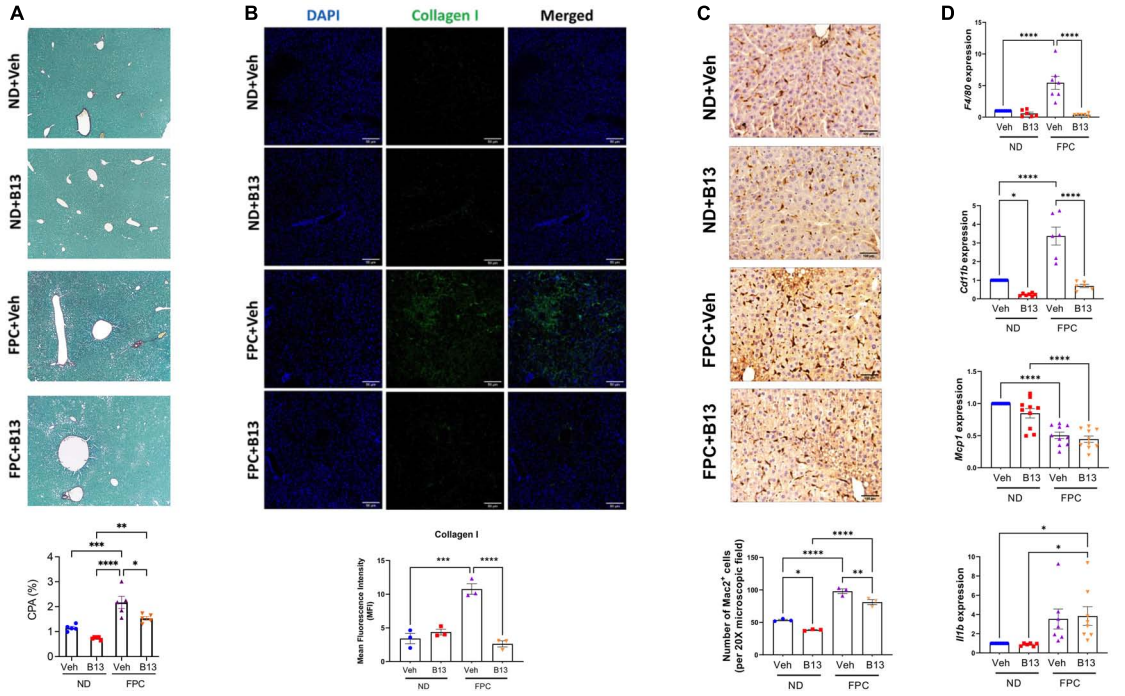

FIGURE 7
Male wild-type mice on FPC diet and administered an acid ceramidase inhibitor developed less fibrosis than vehicle control mice. **(A)** Representative photomicrograph of Sirius red-stained liver sections (top). Sirius red staining was quantified (collagen proportional area, CPA, bottom). **(B)** Representative immunofluorescence images of mouse liver tissue sections stained with DAPI (blue) and collagen 1 (green) (top). Scale bar: 50 μm. Mean fluorescence intensity (MFI) of collagen type 1 was measured in five sections per mouse (N = 3 mice per group) (bottom). **(C)** Representative immunohistochemical images of mouse liver tissue sections stained with Mac2 (top). Scale bar: 50 μm. The number of Mac2 positive cells per 20× microscopic field were measured in five sections per mouse (N = 3 mice per group) (bottom). **(D)** Quantitative reverse transcription polymerase chain reaction (qRT-PCR) quantified expression (mean ± SEM) of the indicated genes, compared using one-way ANOVA with Tukey's method for multiple comparisons. Samples are normalized to *Gapdh*. $^{*}p < 0.05$, $^{**}p < 0.01$, $^{***}p < 0.001$, $^{****}p < 0.0001$.

targeting other aspects of ceramide metabolism has had a varying impact. Overexpression of aCDase in hepatocytes or adipose tissue improves insulin sensitivity in mice receiving a high-fat diet (10), but deficiency in alkaline ceramidase 3 alleviates inflammation and fibrosis in a mouse model of NASH (28). Furthermore, ceramide subspecies have different cell-specific functions: for example, C_{16}-ceramide promotes apoptosis, whereas C_{22}-ceramide and $C_{18:1}$-ceramide inhibit apoptosis in hepatocytes (29, 30). A recent study demonstrated that short-chain C_6-ceramide promotes anti-oxidant signaling in a mouse model of NASH (31). Thus, it is overly simplistic to stipulate that all ceramides are pathologic in NASH or other disease settings.

Our prior studies demonstrate a pivotal role of aCDase in regulating HSC activity and hepatic fibrosis in several systems, including models of NASH (3, 4). For example, treatment with B13 reduced fibrogenesis in precision-cut fibrotic liver slices from CDAHFD-fed rats, and mice with deletion of aCDase in HSCs experienced decreased fibrosis development in this dietary model (4). Furthermore, a signature consisting of the top genes downregulated by ceramide, the CRS, was significantly increased in NAFLD patients with advanced compared to mild fibrosis. This suggests that the transcriptional response associated with increasing fibrosis could be reversed with aCDase inhibition in patients with NAFLD (4). Here, our studies demonstrate that the metabolic parameters of NASH including glucose tolerance, hepatic triglycerides, and steatosis are not significantly altered with HSC depletion or pharmacologic inhibition of aCDase. Taken together, our findings highlight that targeting aCDase has significant antifibrotic effects that are dissociated from metabolic parameters. This suggests that aCDase acts downstream of the initial metabolic perturbations that lead to NASH and most likely at the level of HSCs, which transmit these proximal changes into a fibrotic response.

This work has several limitations. We intentionally selected a therapeutic intervention in which the NASH phenotype was established before treatment with the aCDase inhibitor B13, as this mimics treatment of patients with established disease. However, this timing does not allow for analysis of how targeting aCDase modulates development of steatosis and/or steatohepatitis. We also did not explore how aCDase targeting regulates adipose tissue and insulin signaling, including insulin

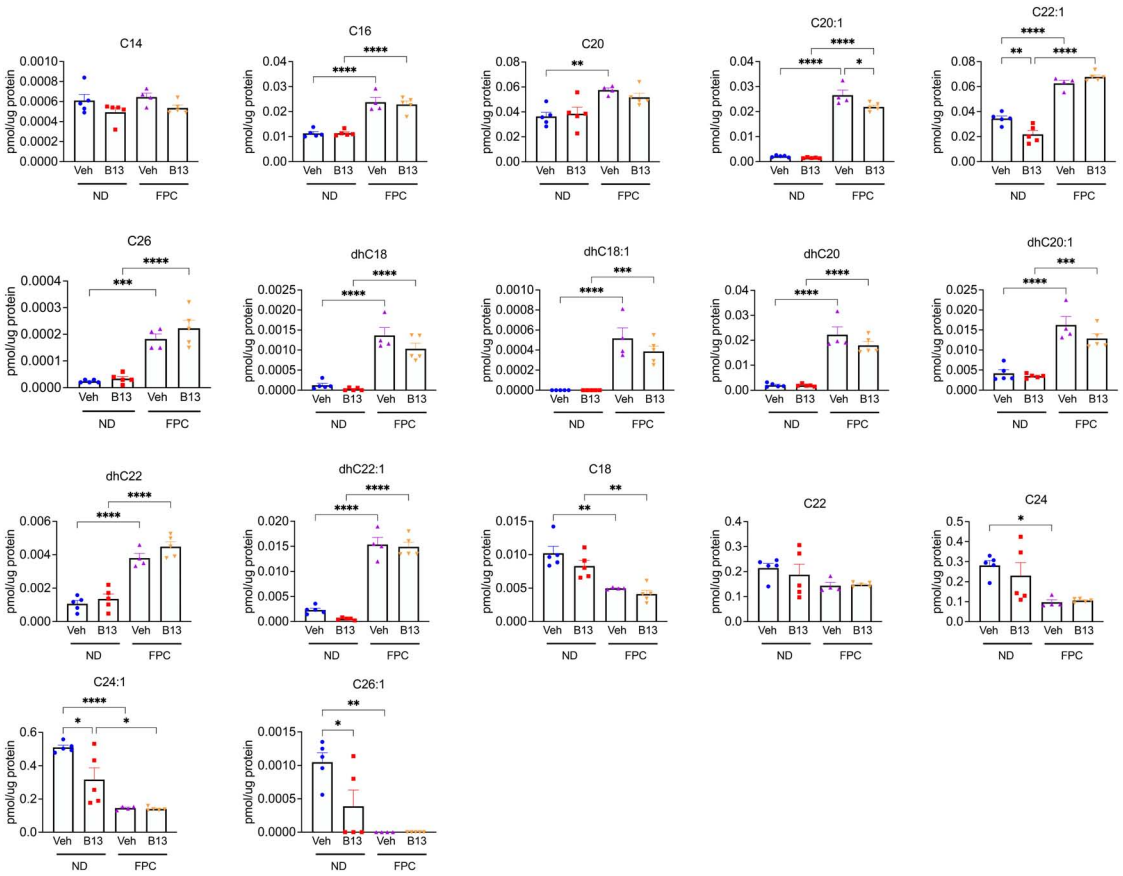

FIGURE 8
Ceramide species were analyzed in male wild-type mice receiving the FPC diet and B13 treatment. Hepatic ceramide subspecies. n = 4–5 mice per group. $^{*}p < 0.05$, $^{**}p < 0.01$, $^{***}p < 0.001$, $^{****}p < 0.0001$.

tolerance. We performed sphingolipid analysis on mouse hepatic tissues following receipt of the FPC diet at two different time points: one following 16 weeks (Figure 5) and one following 12 weeks (Figure 8). We observed that the FPC diet increased C20:1 and C22:1 at both time points and increased additional ceramide subspecies at 12 weeks, including C16, C20, and C26 (Figure 8). The differential results in ceramide subspecies at the two time points suggest that exposure to the FPC diet results in time-dependent changes in sphingolipid profiles. We also observed that the FPC diet induced decreases in several subspecies, further highlighting the diversity of ceramides. Interestingly, B13 treatment modulated levels of C24:1 and C26:1 in mice fed a normal diet and C20:1 in mice fed FPC. We want to highlight that not all ceramides were measured in the analysis. We previously measured sphingolipids in mice receiving systemic B13 in a carbon tetrachloride model of fibrosis: in this study, B13 increased two specific subspecies, C_{26}-ceramide and $C_{26:1}$-ceramide (4), which was not observed in these studies with the FPC model. Additional studies are underway to measure cell-specific changes in sphingolipids, including short-chain ceramides, and to determine whether compensation by other pathways involved in ceramide metabolism occurs with aCDase deletion. Furthermore, we selected two dietary models of NASH, but other dietary or genetic models will be important to include in future studies.

Our findings also highlight potential sex differences in response to the FPC model. Human NASH studies as well as studies on HCC incidence have demonstrated a significant difference in incidence between males and females. Studies have illustrated a clear link between estrogen and the decreased occurrence of HCC (32, 33). The same phenomenon holds true for NASH. Studies have shown that NASH is more prevalent in males and post-menopausal women than pre-menopausal women (34, 35). However, studies investigating NASH fibrosis have been inconclusive in a potential role for sex in its incidence (36–38). In our studies using the FPC model, we observed significant increases in serum insulin levels among male mice receiving the FPC diet compared to the standard chow diet. This difference was not observed among female mice, which is consistent with prior studies demonstrating that female mice are less prone to develop insulin resistance (39).

We acknowledge that the studies were underpowered to comprehensively analyze differences by sex, and future studies are needed to characterize differences in metabolic and sphingolipid parameters with the FPC model.

Conclusion

In summary, our study suggests that targeting aCDase in two dietary models of NASH reduces fibrogenesis without worsening metabolic features. Our findings suggest that this strategy of targeting aCDase may add to the armamentarium of antifibrotic therapies for patients with NASH as well as other types of chronic liver disease.

Data availability statement

The raw data supporting the conclusions of this article will be made available by the authors, without undue reservation.

Ethics statement

The animal study was reviewed and approved by the Institutional Animal Care and Use Committee at the University of California, San Francisco.

Author contributions

JYC and CCD contributed to conception and design of the study. CC, AY, SS, and MS performed the experiments and data analysis. ANM performed the histology assessment. IM and YH performed the sphingolipid analysis. CC, JYC, and CCD wrote sections of the manuscript. All authors contributed to manuscript revision, read, and approved the submitted version.

Funding

The research reported in this publication was supported by the National Institute of Diabetes and Digestive and Kidney Diseases of the NIH under award number K08DK114548 (to JYC) and the UCSF Liver Center P30DK026743 (UCSF Liver Center Pilot/Feasibility grant to JYC). This work was also supported by funds from the UCSF Department of Medicine (to JYC).

Conflict of interest

The authors declare that the research was conducted in the absence of any commercial or financial relationships that could be construed as a potential conflict of interest.

Publisher's note

Author disclaimer

The content is solely the responsibility of the authors and does not necessarily represent the official views of the NIH.

Supplementary material

The Supplementary Material for this article can be found online at: https://www.frontiersin.org/articles/10.3389/fmed.2022.881848/full#supplementary-material

SUPPLEMENTARY FIGURE 1
Female hepatic stellate cell-specific acid ceramidase knockout mice demonstrate no metabolic differences compared to their wild-type counterparts. **(A)** Experimental schematic. Female hepatic stellate cell-specific knockout (cACKO) or control (Ctrl) mice were fed either a normal diet (ND) or Fructose, Palmitate, and Cholesterol (FPC) diet for 16 weeks. **(B)** Measured hepatic triglycerides. **(C)** Liver to body proportional weight in percent. **(D,E)** Glucose tolerance test was performed at 14 weeks and area under the curve (AUC) was determined. **(F)** Measured serum insulin levels. n = 3–5 mice per group. $^{***}p < 0.001$, $^{****}p < 0.0001$.

References

1. Wynn TA. Fibrotic disease and the T(H)1/T(H)2 paradigm. *Nat Rev Immunol.* (2004) 4:583–94. doi: 10.1038/nri1412

2. Angulo P, Kleiner DE, Dam-Larsen S, Adams LA, Bjornsson ES, Charatcharoenwitthaya P, et al. Liver fibrosis, but no other histologic features, is associated with long-term outcomes of patients with nonalcoholic fatty liver disease. *Gastroenterology.* (2015) 149:389–397.e10.

3. Chen JY, Newcomb B, Zhou C, Pondick JV, Ghoshal S, York SR, et al. Tricyclic antidepressants promote ceramide accumulation to regulate collagen production

in human hepatic stellate cells. *Sci Rep.* (2017) 7:44867. doi: 10.1038/srep44867

4. Alsamman S, Christenson SA, Yu A, Ayad NME, Mooring MS, Segal JM, et al. Targeting acid ceramidase inhibits YAP/TAZ signaling to reduce fibrosis in mice. *Sci Transl Med.* (2020) 12:eaay8798. doi: 10.1126/scitranslmed.aay8798

5. Kasumov T, Li L, Li M, Gulshan K, Kirwan JP, Liu X, et al. Ceramide as a mediator of non-alcoholic Fatty liver disease and associated atherosclerosis. *PLoS One.* (2015) 10:e0126910. doi: 10.1371/journal.pone.0126910

6. Kurek K, Piotrowska DM, Wiesiołek-Kurek P, Łukaszuk B, Chabowski A, Górski J, et al. Inhibition of ceramide de novo synthesis reduces liver lipid accumulation in rats with nonalcoholic fatty liver disease. *Liver Int.* (2014) 34:1074–83.

7. Ichi I, Nakahara K, Fujii K, Iida C, Miyashita Y, Kojo S. Increase of ceramide in the liver and plasma after carbon tetrachloride intoxication in the rat. *J Nutr Sci Vitaminol.* (2007) 53:53–6.

8. Xia JY, Morley TS, Scherer PE. The adipokine/ceramide axis: key aspects of insulin sensitization. *Biochimie.* (2014) 96:130–9. doi: 10.1016/j.biochi.2013.08.013

9. Yetukuri L, Katajamaa M, Medina-Gomez G, Seppänen-Laakso T, Vidal-Puig A, Oresic M. Bioinformatics strategies for lipidomics analysis: characterization of obesity related hepatic steatosis. *BMC Syst Biol.* (2007) 1:12. doi: 10.1186/1752-0509-1-12

10. Xia JY, Holland WL, Kusminski CM, Sun K, Sharma AX, Pearson MJ, et al. Targeted Induction of ceramide degradation leads to improved systemic metabolism and reduced hepatic steatosis. *Cell Metab.* (2015) 22:266–78. doi: 10.1016/j.cmet.2015.06.007

11. Eliyahu E, Shtraizent N, Shalgi R, Schuchman EH. Construction of conditional acid ceramidase knockout mice and in vivo effects on oocyte development and fertility. *Cell Physiol Biochem.* (2012) 30:735–48. doi: 10.1159/000341453

12. Henderson NC, Arnold TD, Katamura Y, Giacomini MM, Rodriguez JD, McCarty JH, et al. Targeting of alphav integrin identifies a core molecular pathway that regulates fibrosis in several organs. *Nat Med.* (2013) 19:1617–24. doi: 10.1038/nm.3282

13. Wang X, Zheng Z, Caviglia JM, Corey KE, Herfel TM, Cai B, et al. Hepatocyte TAZ/WWTR1 promotes inflammation and fibrosis in nonalcoholic steatohepatitis. *Cell Metab.* (2016) 24:848–62.

14. Folch J, Lees M, Sloane Stanley GH. A simple method for the isolation and purification of total lipides from animal tissues. *J Biol Chem.* (1957) 226:497–509.

15. Pickens MK, Yan JS, Ng RK, Ogata H, Grenert JP, Beysen C, et al. Dietary sucrose is essential to the development of liver injury in the methionine-choline-deficient model of steatohepatitis. *J Lipid Res.* (2009) 50:2072–82. doi: 10.1194/jlr.M900022-JLR200

16. Kleiner DE, Brunt EM, Van Natta M, Behling C, Contos MJ, Cummings OW, et al. Design and validation of a histological scoring system for nonalcoholic fatty liver disease. *Hepatology.* (2005) 41:1313–21.

17. Bielawska A, Linardic CM, Hannun YA. Ceramide-mediated biology. Determination of structural and stereospecific requirements through the use of N-acyl-phenylaminoalcohol analogs. *J Biol Chem.* (1992) 267:18493–7.

18. Raisova M, Goltz G, Bektas M, Bielawska A, Riebeling C, Hossini AM, et al. Bcl-2 overexpression prevents apoptosis induced by ceramidase inhibitors in malignant melanoma and HaCaT keratinocytes. *FEBS Lett.* (2002) 516:47–52. doi: 10.1016/s0014-5793(02)02472-9

19. Bielawska A, Bielawski J, Szulc ZM, Mayroo N, Liu X, Bai A, et al. Novel analogs of D-e-MAPP and B13. Part 2: signature effects on bioactive sphingolipids. *Bioorg Med Chem.* (2008) 16:1032–45. doi: 10.1016/j.bmc.2007.08.032

20. Bai A, Szulc ZM, Bielawski J, Pierce JS, Rembiesa B, Terzieva S, et al. Targeting (cellular) lysosomal acid ceramidase by B13: design, synthesis and evaluation of novel DMG-B13 ester prodrugs. *Bioorg Med Chem.* (2014) 22:6933–44.

21. Selzner M, Bielawska A, Morse MA, Rüdiger HA, Sindram D, Hannun YA, et al. Induction of apoptotic cell death and prevention of tumor growth by ceramide analogues in metastatic human colon cancer. *Cancer Res.* (2001) 61:1233–40.

22. Samsel L, Zaidel G, Drumgoole HM, Jelovac D, Drachenberg C, Rhee JG, et al. The ceramide analog, B13, induces apoptosis in prostate cancer cell lines and inhibits tumor growth in prostate cancer xenografts. *Prostate.* (2004) 58:382–93. doi: 10.1002/pros.10350

23. Hannun YA, Obeid LM. Many ceramides. *J Biol Chem.* (2011) 286:27855–62.

24. Martínez L, Torres S, Baulies A, Alarcón-Vila C, Elena M, Fabriàs G, et al. Myristic acid potentiates palmitic acid-induced lipotoxicity and steatohepatitis associated with lipodystrophy by sustaning de novo ceramide synthesis. *Oncotarget.* (2015) 6:41479–96. doi: 10.18632/oncotarget.6286

25. Chaurasia B, Tippetts TS, Mayoral Monibas R, Liu J, Li Y, Wang L, et al. Targeting a ceramide double bond improves insulin resistance and hepatic steatosis. *Science.* (2019) 365:386–92. doi: 10.1126/science.aav3722

26. Martel C, Esposti DD, Bouchet A, Brenner C, Lemoine A. Non-alcoholic steatohepatitis: new insights from OMICS studies. *Curr Pharm Biotechnol.* (2012) 13:726–35.

27. Puri P, Wiest MM, Cheung O, Mirshahi F, Sargeant C, Min HK, et al. The plasma lipidomic signature of nonalcoholic steatohepatitis. *Hepatology.* (2009) 50:1827–38.

28. Wang K, Li C, Lin X, Sun H, Xu R, Li Q, et al. Targeting alkaline ceramidase 3 alleviates the severity of nonalcoholic steatohepatitis by reducing oxidative stress. *Cell Death Dis.* (2020) 11:28.

29. Stiban J, Perera M. Very long chain ceramides interfere with C16-ceramide-induced channel formation: A plausible mechanism for regulating the initiation of intrinsic apoptosis. *Biochim Biophys Acta.* (2015) 1848:561–7. doi: 10.1016/j.bbamem.2014.11.018

30. Raichur S, Wang ST, Chan PW, Li Y, Ching J, Chaurasia B, et al. CerS2 haploinsufficiency inhibits beta-oxidation and confers susceptibility to diet-induced steatohepatitis and insulin resistance. *Cell Metab.* (2014) 20:919.

31. Zanieri F, Levi A, Montefusco D, Longato L, De Chiara F, Frenguelli L, et al. Exogenous liposomal ceramide-C6 ameliorates lipidomic profile, energy homeostasis, and anti-oxidant systems in NASH. *Cells.* (2020) 9:1237.

32. Li Y, Li H, Spitsbergen JM, Gong Z. Males develop faster and more severe hepatocellular carcinoma than females in kras(V12) transgenic zebrafish. *Sci Rep.* (2017) 7:41280. doi: 10.1038/srep41280

33. O'Brien MH, Pitot HC, Chung SH, Lambert PF, Drinkwater NR, Bilger A. Estrogen receptor-alpha suppresses liver carcinogenesis and establishes sex-specific gene expression. *Cancers.* (2021) 13:2355. doi: 10.3390/cancers13102355

34. Lonardo A, Nascimbeni F, Ballestri S, Fairweather D, Win S, Than TA, et al. Sex differences in nonalcoholic fatty liver disease: state of the art and identification of research gaps. *Hepatology.* (2019) 70:1457–69. doi: 10.1002/hep.30626

35. Long MT, Pedley A, Massaro JM, Hoffmann U, Ma J, Loomba R, et al. A simple clinical model predicts incident hepatic steatosis in a community-based cohort: the Framingham heart study. *Liver Int.* (2018) 38:1495–503. doi: 10.1111/liv.13709

36. Caballería L, Pera G, Arteaga I, Rodríguez L, Alumà A, Morillas RM, et al. High prevalence of liver fibrosis among european adults with unknown liver disease: a population-based study. *Clin Gastroenterol Hepatol.* (2018) 16:1138–1145.e5

37. Kim D, Kim WR, Kim HJ, Therneau TM. Association between noninvasive fibrosis markers and mortality among adults with nonalcoholic fatty liver disease in the United States. *Hepatology.* (2013) 57:1357–65.

38. Tanaka K, Takahashi H, Hyogo H, Ono M, Oza N, Kitajima Y, et al. Epidemiological survey of hemoglobin A1c and liver fibrosis in a general population with non-alcoholic fatty liver disease. *Hepatol Res.* (2019) 49:296–303. doi: 10.1111/hepr.13282

39. Reynolds TH, Dalton A, Calzini L, Tuluca A, Hoyte D, Ives SJ. The impact of age and sex on body composition and glucose sensitivity in C57BL/6J mice. *Physiol Rep.* (2019) 7:e13995. doi: 10.14814/phy2.13995